High-Pressure Studies of 1,3,5,7-Cyclooctatetraene: Experiment and Theory

Sergey N. Tkachev,[†] Michael Pravica,*[,†] Eunja Kim,[†] Edward Romano,[†] and Philippe F. Weck[‡]

Department of Physics and Astronomy, and High Pressure Science and Engineering Center, University of Nevada Las Vegas, 4505 Maryland Parkway, Las Vegas, Nevada 89154-4002, and Department of Chemistry, University of Nevada Las Vegas, 4505 Maryland Parkway, Las Vegas, Nevada 89154-4003

Received: August 5, 2008; Revised Manuscript Received: September 9, 2008

High-pressure studies of 1,3,5,7-cyclooctatetraene have been performed by using Raman spectroscopy up to 16 GPa and compared with complementary density functional calculations. Angular-dispersive X-ray diffraction studies were also performed in the solid state at elevated pressure. The lattice constants of solid 1,3,5,7-cyclooctatetraene obtained from the X-ray diffraction pattern taken at 3.8 GPa and room temperature are in good agreement with theoretical results. At least two phase transitions were observed during pressure increase followed by the loss of long-range crystallographic order, which was also associated with a strong pressure-induced luminescence that allowed estimation of band gap alterations with pressure.

Introduction

Hydrocarbons represent relatively simple molecular systems that are tremendously vital to our society due to their high energy content, foundation of roads and roofs (asphalt, tar, etc.), lubrication properties, and use in plastics and other polymers.[1] There are some estimates that polycyclic aromatic hydrocarbons (PAHs) may represent a significant fraction of mass in the universe in the form of interstellar matter.[2,3] This would not be unreasonable due to the fact that carbon synthesized from nuclear fusion in stars would likely react with hydrogen (the most abundant element in the Universe) to form hydrocarbons. Of these, aromatic hydrocarbons are considered to be very chemically stable. There may be large amounts of hydrocarbons such as methane[4] and even benzene[5] on moons such as Titan, which may have originated from deep underneath the moon's surface as proposed for methane.[6] As many of these compounds probably exist under conditions dramatically different from ambient conditions, it would be highly useful to study hydrocarbons under extreme conditions. Beyond this, the hydrocarbons that are present in the Earth were mostly created under high-pressure and high-temperature conditions. It is thus our desire to study the behavior of hydrocarbons—particularly cyclic hydrocarbons under extreme conditions.

We have studied saturated[7] and aromatic[8] hydrocarbons, and, in this study, an interesting hydrocarbon, which is neither aromatic nor antiaromatic:[9] 1,3,5,7-cyclooctatetraene (COT). COT (C_8H_8) is a ringed, conjugated aliphatic molecule that is not subject to the $4n + 2$ Hückel's rule[1] and thus is not planar but rather tub shaped despite the sp^2 hybridization of the molecules[10] (Figure 1). As a consequence of this geometrically frustrated state, the molecule is highly reactive and less thermodynamically stable than aromatic molecules such as benzene.[11] It is believed that a derivative of COT transforms into polymorphs of itself (ring inversion[12]) by temporarily adopting either the planar D_{4h} symmetry (conjugated) or the planar D_{8h} symmetry (ring structure) as an intermediate state between tub-shaped/puckered conformations[12] which are D_{2d} symmetry.[11,13] COT will aromatize with single or double electron transfer (by, e.g., reacting it with potassium[14] or uranium[15]) to form COT^{-} [16] or COT^{2-}.[17,18] In this state, the anion and dianion now satisfy Hückel's rule and are planar with equal C−C bond lengths.[16,17]

Due to the relative ease with which the planarization of the molecule can occur, we sought to determine if pressure would have a similar role by increasing intermolecular interactions via decrease in intermolecular distance: either by distorting the molecule to physically planarize it (and create a quantum mechanically degenerate resonance electronic state) or to induce electron transfer to and from other molecules. Beyond this, much could be learned about the intermediate state that exists during ring inversion by using pressure as a thermodynamic variable. As the complex chemistry and physics of aromatic and antiaromatic molecules is yet to be fully understood, and is of great interest to chemists, application of pressure to induce bonding transformations can aid in understanding the nature of these two types of hydrocarbons. With increased intermolecular density, there is also a likelihood of polymerizing and/or dimerizing molecules. Thus, studies of the behavior of hydrocarbons (particularly reactive ones such as COT) with pressure will be beneficial to polymer chemistry in the desire to create novel routes for polymeric synthesis or even perhaps finding a route to breaking down polymers into hydrocarbon constituents in reverse.

In this paper, besides the abovementioned attempt to explore the possibility of pressure-induced aromatization, we examined the high-pressure phase diagram of COT, which is the first such effort ever conducted to the best of our knowledge. Though aromatic, cyclic benzene (C_6H_6) has been extensively studied at high pressure,[19−23] cyclic COT, which is neither aromatic nor antiaromatic, has not. For this study, the primary tools of investigation have been Raman spectroscopy and X-ray diffraction. These methods and infrared spectroscopy have been extensively employed to study COT at room pressure[24−26] and form a basis for initial comparisons. Though some of the new Raman bands appearing in the presented Raman spectra are due to the pressure-induced changes in COT and have only tentative assignments, phase boundaries and chemical reactions in COT under pressure can be clarified. Potential planarization and

* Corresponding author. E-mail: pravica@physics.unlv.edu.
[†] Department of Physics and Astronomy.
[‡] Department of Chemistry.

10.1021/jp806968c CCC: $40.75
Published on Web 10/18/2008

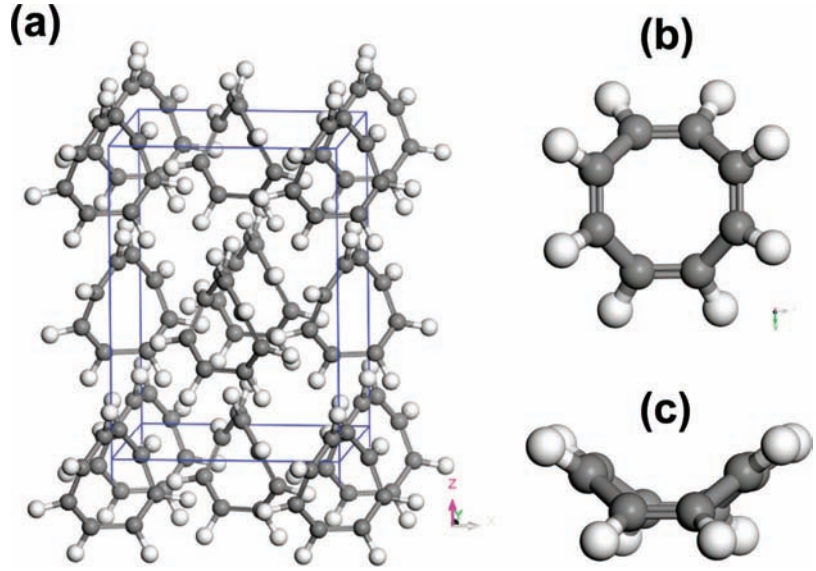

Figure 1. (a) The orthorhombic cyclooctatetraene crystal structure (space group *Aba*2) and the D_{2d} symmetry conformer of the COT molecule: (b) top view and (c) side view.

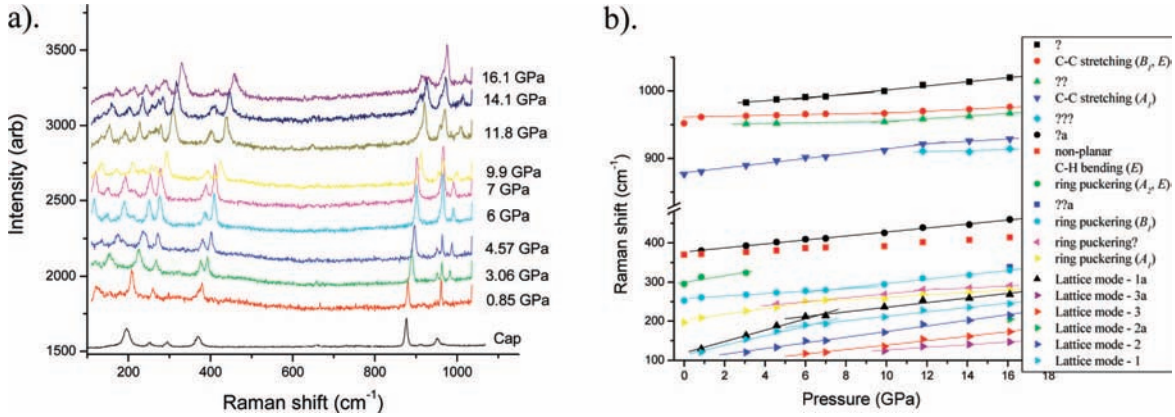

Figure 2. (a) Raman spectra of COT in the 100−1080 cm^{-1} frequency region (Cap stands for measurements in a capillary, i.e., at room pressure); (b) pressure dependence of Raman modes in the same frequency region. Unassigned (or tentatively assigned) Raman bands as well as pressure dependencies of Raman bands that either change their slopes or appear or disappear are indicated by question marks and solid lines, accordingly.

polymerization of COT with pressure are both given consideration during descriptions of Raman spectral evolution with pressure.

Experimental Techniques and Computational Methods

A diamond anvil cell, or DAC (Mao-Bell type), with 300-μm diamond culets was used in this study to generate pressures up to 16 GPa. A liquid sample of COT (obtained from Aldrich chemical with 98% purity) was manually loaded into the sample chamber (with a diameter of about 100 μm), which was drilled in a rhenium gasket that was initially preindented to about 80 μm from 250 μm initial thickness. A thermally annealed ruby sphere (the size of about 5−10 μm) was placed in the sample chamber (prior to sample loading) and constituted the pressure sensor.[27]

For the optical studies of COT, Raman spectroscopy was performed. The experimental setup consisted of a multiline Ar-ion laser (488 nm as well as 514.5 nm wavelength), with an output of about 5−10 mW of laser power incident on the sample (with a 10-μm diameter focused spot), a plasma line holographic transmission grating filter, focusing and collimating external optics, notch filters, a fully automated imaging spectrometer (ISA HR 460), and a Peltier-cooled CCD detector. Typical acquisition times of the spectra collected by using backscattering geometry were within 20 s. During the accumulation cycle, which was controlled by two PC-based programs (WinSpec/32 and WizSpec), the width of the entrance slit in the spectrometer was maintained at 30 μm. Peak positions, widths, and intensities have been determined by using Lorentzian function curve-fitting of the Raman bands.

For the X-ray diffraction studies of COT, a monochromatic synchrotron X-ray beam (with $\lambda = 0.36121$ Å) from the 16ID-B undulator beamline of the High Pressure Collaborative Access Team, Sector 16, at the Advanced Photon Source of Argonne National Laboratory was used. This is also where the Raman spectroscopic studies were performed. A complementary X-ray angular-dispersive powder diffraction study of COT at ~3.8 GPa was performed and, after decompression (from 21 GPa), at ~6 GPa. The equation of state was not determined in this study, due to the limited number of pressure points. The angle dispersive X-ray diffraction patterns were accumulated on a MAR345 image plate detector and integrated in θ, using the Fit2D software package[28] for further processing with MDI's Jade (Materials Data, Inc. Jade: XRD Pattern Processing, Identifica-

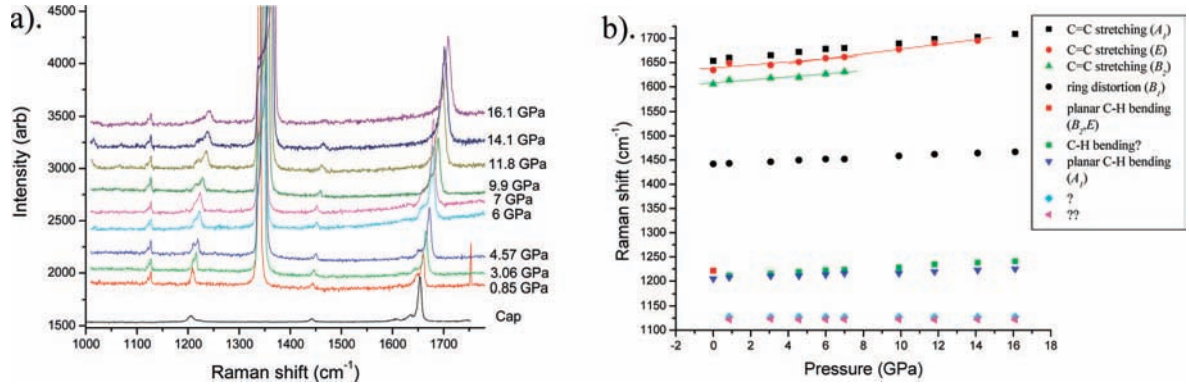

Figure 3. Raman spectra of COT (a) and pressure dependence of assigned Raman modes (b) in the 1000−1780 cm^{-1} frequency region. Cap stands for measurements in a capillary, i.e., at room pressure. Unassigned (or tentatively assigned) Raman bands as well as pressure dependencies of Raman bands that either change their slopes or appear or disappear are indicated by question marks and solid lines, accordingly.

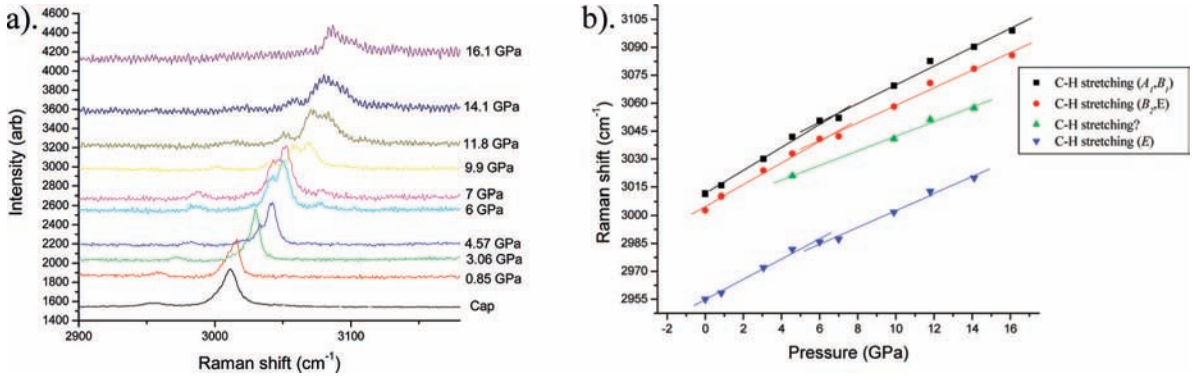

Figure 4. Raman spectra of COT (a) and pressure dependence of Raman modes (b) in the 2900−3180 cm^{-1} frequency region. Cap stands for measurements in a capillary, i.e., at room pressure. Unassigned (or tentatively assigned) Raman bands as well as pressure dependencies of Raman bands that either change their slopes or appear or disappear are indicated by question marks and solid lines, accordingly.

tion, and Quantification, 1995−2006) and PowderCell[29] software to extract structural parameters.

First-principles calculations of the total energies, optimized geometries, and vibrational properties were performed by using the all-electron spin-polarized density functional theory (DFT) implemented in the DMol software[30] and the DFT implementation of the Gaussian 03 computer code.[31] In both sets of calculations, the exchange correlation energy was calculated by using the generalized gradient approximation (GGA) with the parametrization of Perdew and Wang[32] (PW91). Recent calculations on benzene molecules showed that the PW91 functional satisfactorily reproduces structures and energies obtained at the second-order Møller−Plesset (MP2) and coupled-cluster (CCSD(T)) levels of theory.[33] Double numerical basis sets including polarization functions on all atoms, i.e., 6-31G** and DNP basis sets, were used in the Gaussian 03 and Dmol calculations, respectively. The DNP basis set corresponds to a double-ζ quality basis set with d-type polarization functions added to atoms heavier than hydrogen. The DNP basis set is comparable to 6-31G(d,p) Gaussian basis sets[34] with a better accuracy for a similar basis set size.[30,35] In the generation of the numerical basis sets, a global orbital cutoff of 3.7 Å was used. The energy tolerance in the self-consistent field calculations was set to 10^{-6} hartree. Optimized geometries were obtained by using direct inversion in a subspace method (DIIS) with an energy convergence tolerance of 10^{-5} hartree, and a gradient convergence of 2×10^{-3} hartree/Å. DFT calculations were performed for an isolated molecule and a single crystal of cyclooctatretraene (COT). The unit cell used in our calculations to model the crystal structure contained four C_8H_8 molecules, i.e., 64 atoms/unit cell. The Monkhorst−Pack special k-point scheme[36] was used for structural optimizations and electronic properties calculations with a $3 \times 3 \times 2$ mesh to sample the Brillouin zone. For the sake of comparison with experimental data, normal vibrational modes of one COT molecule were also calculated. Starting from the relaxed geometry of a given model structure, the Hessian matrix was constructed by using finite differences of the analytic gradient of the energy with respect to the atomic positions. The vibrational frequencies were obtained by matrix diagonalization of the resulting Hessian matrix in mass-weighted Cartesian coordinates. In turn, diagonalization of the Cartesian matrix yielded the vibrational normal modes.

Ab initio molecular-dynamics simulations were also carried out with use of the Parrinello−Rahman NPT method[37] implemented in the CPMD code[37] to investigate the intriguing structural changes of solid COT under pressure. The ionic and electronic forces were derived separately from an effective Lagrangian based on the PBE GGA exchange correlation functional.[38] Normconserving pseudopotentials were used to treat the interaction between valence and core electrons.[39] Kinetic energy cutoff was 80 Ry with only the γ-point utilized for k-point sampling. The simulations were performed for 2.1 ps in a periodic box starting from the lattice constants and atomic positions at $P = 0$ GPa and $T = 0$ K. The time step of the ionic motion and the fictitious mass of the electronic degrees of freedom were 5 au (0.1 fs) and 1300 au, respectively. The average temperature was set by initializing the kinetic energy and then rescaling the velocities of the atoms whenever the instantaneous temperature deviated from the target temperature by more than 20%. This theoretical approach was used successfully in previous studies.[40,41]

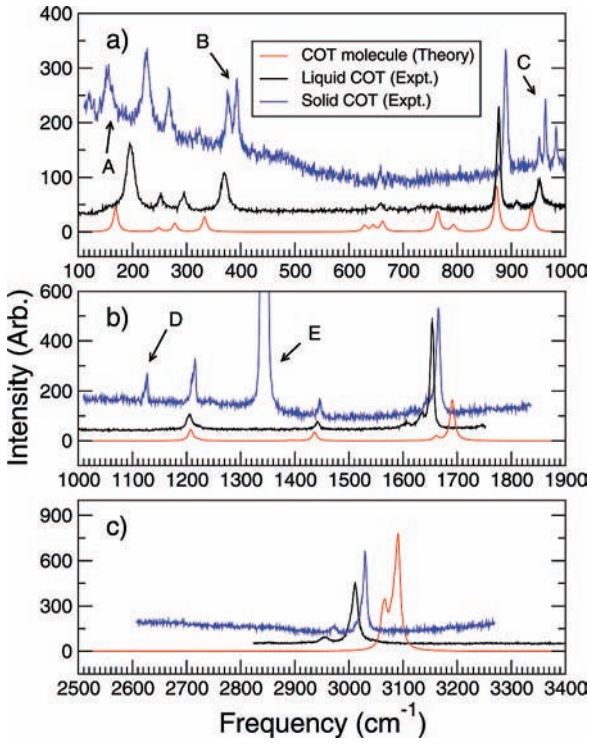

Figure 5. Raman spectra of COTs in gaseous, liquid, and solid phases: (a) in the 100−1000 cm^{-1} frequency region, (b) in the 1000−1900 cm^{-1} frequency region, and (c) in the 2500−3400 cm^{-1} frequency region.

Results and Discussion

The symmetry of the most stable COT molecule conformer is D_{2d} and solid COT is characterized by an orthorhombic crystal lattice, with Schoenflies space group *Aba*2 (Hermann-Mauguin space group C_{2v}^{17}) (cf. Figure 1). Four molecules are in the unit cell. The calculated lattice parameters at 0 K and 0 GPa are $a = 7.864$ Å, $b = 7.849$ Å, and $c = 10.967$ Å from GGA and $a = 7.464$ Å, $b = 7.450$ Å, and $c = 10.409$ Å from the local density approximation (LDA). Both are in good agreement with the experimental values of $a = 7.664$ Å, $b = 7.650$ Å, and $c = 10.688$ Å at 129 K, respectively.[25]

Figure 2 (panels a and b) represents changes in Raman spectra in the 100 to 1080 cm^{-1} frequency range. Five modes in this range are marked with question marks and have never been observed in COT prior to our studies, so their assignments (if any) are speculative (Figure 2b). There are also 6 new modes that are assigned as lattice modes. However, the lattice dynamics of COT crystals have not been studied with the theoretical calculations in this work. There is, however, some ground for tentative assignment of some of these novel modes to twist-boat planarization and boat-to-boat planarization modes observed in 1,3,5-cyclooctatriene with resonance Raman spectroscopy.[42]

Practically all lines in the 100−1080 cm^{-1} region change their slopes, appear, or disappear due to the pressure increase (Figure 2b). The paucity of data does not allow precise identification of pressures at which possible phase transformations occur. However, it is feasible to predict the regions of stability and the regions of pressure-induced transitions. It should also be emphasized that only single crystal X-ray diffraction data can provide an unambiguous identification of a specific type of phase transition observed in COT. The apparent onset of the phase transition from the liquid to solid state of COT can be associated with the appearance of new Raman bands (120 and 129 cm^{-1}) at about 0.85 GPa. The weakening and disappearance of a ring puckering mode (*E* species) alongside the appearance of two new bands near C−C stretch (*E* species) and a new band at 120 cm^{-1} at pressures about 3 GPa (Figure 2b) most likely signify completion of the liquid-to-solid phase transition, unless it is the boundary of a solid−solid phase transition (in this case, the apparent onset of the liquid−solid phase transition will be the actual phase boundary between the liquid and the solid COT), which will be better resolved if smaller increases in pressure are made which can be difficult using a diamond anvil cell.

Another pressure region where changes in slopes of pressure dependencies of major Raman bands as well as the appearance of new bands occur lies between 6 and 12 GPa. This is a relatively broad transition region (Figure 2b). It is most likely indicative of a smeared type of solid-to-solid phase transition in COT and is associated with the following major features: (i) change in slope of the pressure dependence of a new (higher frequency) Raman band near the C−C stretching (*E*) frequency at about 8 GPa; (ii) change in slope of the pressure dependence of the C−C stretching mode (*E*) at about 10 GPa; (iii) change in slope of the pressure dependence of a new (lower frequency) Raman band near the C−C stretching (*E*) mode at about 10 GPa; (iv) change in slope of the pressure dependence of the C−C stretching mode (A_1) at about 12 GPa accompanied by the appearance of a new (lower frequency) band nearby at about 12 GPa; (v) change in slope of the pressure dependence of the ring puckering mode (B_1) at about 7 GPa; (vi) change in slope of the pressure dependence of the ring puckering mode (A_1) at about 6.5 GPa accompanied by a change in slope of the pressure dependence of a new (higher frequency) band nearby at about 12 GPa; and (vii) change in slope of the pressure dependence of two new lattice modes at about 6.5 GPa accompanied by the appearance of a new lattice mode (124 cm^{-1}) at about 10 GPa.

The frequency region between 1000 and 1780 cm^{-1} also contains pressure-induced changes associated with the above-mentioned transition regions. However, these changes are not as dramatic as in the 100−1080 cm^{-1} region when considered from the standpoint of Raman peak positions (Figure 3a,b). The main features associated with the proposed phase transitions are related to the change in slope of pressure dependence of the C═C stretching mode (*E*) at about 6 GPa and the gradual weakening as well as subsequent disappearance of the C═C stretching mode (B_2) at about 7 GPa.

Figure 4a exhibits the Raman spectra of COT in the C−H stretching modes region. There are only three major bands in this frequency region. One new Raman band appears at about 5 GPa (Figure 4b), while the other three bands each change the slope of their pressure dependencies at about 6 GPa in accordance with the proposed second region of a solid−solid phase transition in COT.

It is possible that this second transition region is also a combination of two solid−solid phase transitions with the middle region being a stability field of a second solid phase of COT. However, the Raman data alone cannot provide sufficient constraints to support this possible scenario. Besides additional X-ray diffraction measurements, Brillouin scattering spectroscopy measurements of COT at high pressures will be able to uniquely identify the nature[43,44] and the number of the pressure-induced phase transitions.

In addition to the experimental measurements, Raman active modes were calculated for a single COT molecule by using the PW91 functional as shown in Figure 5, which are in excellent agreement with the previous results.[24] A direct comparison between theoretical results and the experimental Raman spectra

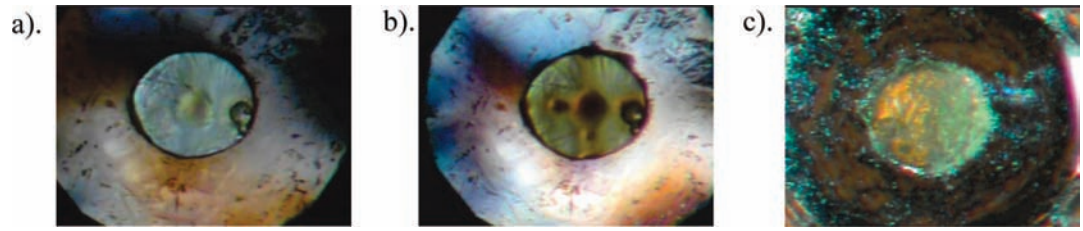

Figure 6. (a) Damage to the COT sample created by a 488 nm laser line. (b) Damage created by a white X-ray synchrotron beam. (c) Sample recovered after compression to 16.1 GPa.

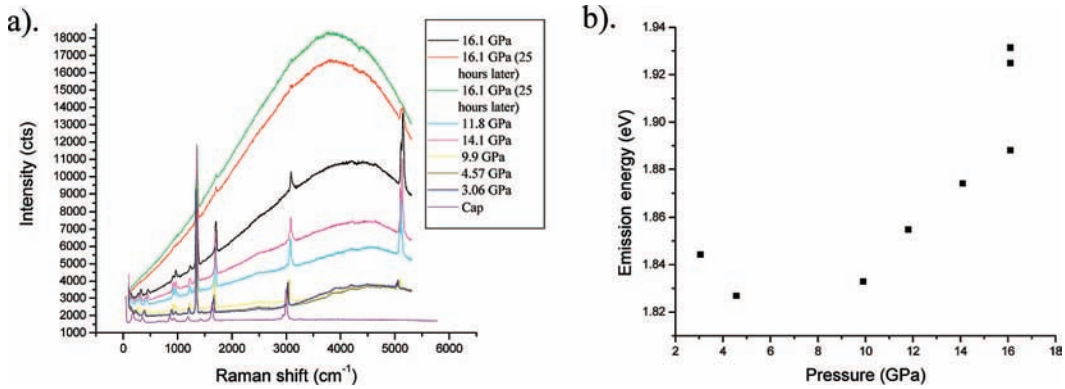

Figure 7. (a) Pressure-induced luminescence; (b) pressure dependence of the luminescence.

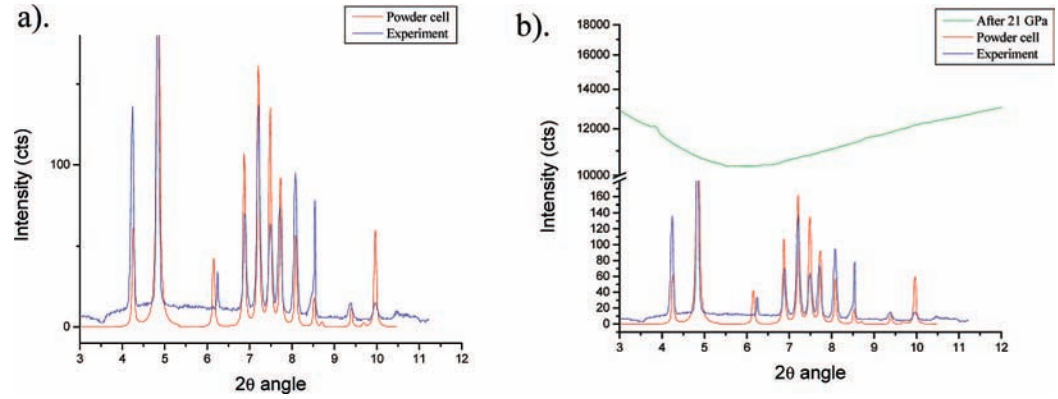

Figure 8. (a) Experimental and calculated X-ray diffraction patterns at 3.8 GPa; (b) comparison between X-ray diffraction patterns at 3.8 and 6 GPa (after decompression from 21 GPa).

indicates that (i) the molecular vibrational modes are nearly intact in both liquid COT taken at $P = 0$ GPa and solid COT taken at $P = 3.06$ GPa, (ii) a slight frequency shift is observed as shown in Figure 5a−c, and (iii) the vibrational mode below 200 cm^{-1} as indicated by "A" in Figure 5a is likely a lattice mode in solid COT as it does not appear in molecular and liquid COT. A significant change is observed in the modes indicated as "B" and "C" due to intermolecular interactions in solid COT. The origin of the mode indicated as "D" is unclear. The mode indicated as "E" is from the diamonds in the diamond anvil cell.

It is important to emphasize that at 16.1 GPa, after about 25 h, the signal-to-noise ratio for all of the Raman peaks of COT became very poor due to the appearance of a strong background associated with luminescence excited by 514.5 nm as well as 647.1 nm lasers. On the other hand, the 488 nm laser line and the white X-ray synchrotron beam from an energy-dispersive X-ray diffraction experiment (not reported here) both created visible damage to COT samples (Figure 6a,b), and the area of damage also emits strong luminescence when probed by 514.5 and 647.1 nm lasers. Upon decompression of the DAC, the resulting product of irreversible pressure-induced chemical reaction was recovered (Figure 6c) and appears gel-like.

Pressure-induced luminescence of COT (Figure 7a) experiences a well-pronounced increase in intensity and blue shifts (Figure 7b) above ~10 GPa. Even though this behavior might be an indication of indirect→direct band crossing that is followed by a widening of the direct band gap under compression, the only way to fully interpret this phenomenon is to perform a series of electronic band structure calculations and also to complement them with high-pressure optical absorption measurements. After 25 h at 16.1 GPa, the luminescence intensity increased even more dramatically and was accompanied by a more than 43-meV widening of the band gap (Figure 7, panels a and b).

X-ray Diffraction Results

We indexed our X-ray powder diffraction pattern taken at 3.8 GPa using Jade. The pattern was most easily indexed by using orthorhombic unit cell symmetry with space group No. 41, *Aba*2. The derived lattice constants were $a = 6.73(1)$ Å, $b = 6.726(3)$ Å, and $c = 9.72(1)$ Å, with unit cell volume $V = 440(1)$ $Å^3$ (Figure 8a). We have carried out ab initio molecular dynamics simulations to investigate the intriguing structural change of solid COT under pressure. The resulting lattice

constants were $a = 6.814$ Å, $b = 6.993$ Å, and $c = 9.859$ Å at $P = 3.8$ GPa and $T = 300$ K, in excellent agreement with the experimental values presented in this study. Our ab initio molecular dynamics study at $P = 0.0$ GPa and $T = 129$ K also results in the theoretical lattice constants of $a = 7.733$ Å, $b = 7.66$ Å, and $c = 10.855$ Å, in excellent agreement with experimental values.[25]

Although the X-ray beam was rastered over the area of the sample during the data accumulation to improve the quality of the powder diffraction patterns, atomic positions in solid COT were not constrained in this study because of the relatively large size (when compared with the X-ray beam focal point dimensions at the sample) of crystallites formed at pressure and their possible preferred orientation. After pressurizing the sample to 21 GPa and decompressing it to 6 GPa, no X-ray diffraction pattern was observed in the quenched product, implying that long-range structural order has been lost (Figure 8b).

To the best of our knowledge, this is the first reported high-pressure study of COT. Even though previous measurements of COT with X-ray diffraction (XRD), Raman, and IR spectroscopy were able to constrain crystallographic structure and vibrational mode assignments in the low temperature, ambient pressure solid phase as well as in the liquid (Raman/IR) phase, pressure-induced transformations remained unexplored in those studies. The present Raman and X-ray diffraction results provide strong evidence of at least two pressure-induced phase transitions followed by a complete loss of long-range structural order and resulting in a transformation of COT to a more stable, higher in density, cross-linked dimer, and/or polymer with reduced number of unsaturated bonds.[45] Single crystal studies in the DAC will be needed to carry out a more thorough X-ray diffraction study to constrain the atomic positions in COT at high pressures.

Conclusions

In summary, we have conducted high-pressure studies of solid 1,3,5,7-cyclooctatetraene using Raman spectroscopy up to 16 GPa and compared our results to density functional calculations. A complementary X-ray diffraction pattern taken at 3.8 GPa shows that the crystalline symmetry of the solid 1,3,5,7-cyclooctatetraene is orthorhombic with the space group *Aba*2, which is the same unit cell symmetry as the low-temperature ambient pressure solid. Lattice constants extracted from XRD analysis are $a = 6.73(1)$ Å, $b = 6.726(3)$ Å, and $c = 9.72(1)$ Å, which are in good agreement with theoretical results (6.814 Å, 6.993 Å, 9.859 Å). We also found that solid COT undergoes structural changes under pressure, followed by the loss of the long-range crystallographic order and, presumably, formation of a more stable and denser cross-linked species. Further studies are required to fully constrain the atomic positions of solid COT under pressure and determine the nature of the polymerized or dimerized product. Luminescence measurements have indicated that COT may undergo indirect→direct band crossing under pressure. Strong luminescence observed in the Raman spectra at 16 GPa allows us to roughly estimate the band gap of this organic solid. A newly synthesized COT product of the pressure-induced chemical reaction is stable at ambient conditions and, due to its band gap width, might have potential wide bandgap semiconductor applications.

Acknowledgment. We thank Malcolm Nicol for useful initial discussions and Prof. Oliver Tschauner and Francisco Sermeno for aid in the measurements. We are grateful to the HPCAT staff for their technical assistance, particularly Stas Sinogeikin. Use of the Advanced Photon Source was supported by the U.S. Department of Energy, Office of Science, Office of Basic Energy Sciences, under Contract No. DE-AC02-06CH11357. We gratefully acknowledge support from the U.S. Department of Energy Cooperative Agreement No. DE-FC08-01NV14049 with the University of Nevada Las Vegas and support from the U.S. Army via RDECOM ACQ CTR Contract W9011NF-05-1-0266 and the DOE DE-FC8806NA27684 Cooperative Agreements with UNLV. We thank the NASA/Nevada Space grant for largely supporting this work. One of us (M.P.) wishes to thank Prof. Walter Pravica for initial discussions leading to the idea of pressure-induced aromatization.

Supporting Information Available: Complete citations for refs 4 and 31. This material is available free of charge via the Internet at http://pubs.acs.org.

References and Notes

(1) Wade, L. G., Jr. *Organic Chemistry*, 5th ed.; Prentice Hall: Upper Saddle River, NJ, 2003.
(2) Leger, A.; d'Hendecourt, L.; Defourneau, D. *Astron. Astrophys.* **1989**, *216*, 148–164.
(3) Bohme, D. K. *Chem. Rev.* **1992**, *92*, 1487–1508.
(4) Stofan, E. R.; et al. *Nature* **2007**, *445*, 61–64.
(5) Vuitton, V.; Yelle, R. V.; Cui, J. *J. Geophys. Res.* **2008**, *113*, E05007.
(6) Tobie, G.; Lunine, J. I.; Sotin, C. *Nature* **2006**, *440*, 61–64.
(7) Pravica, M.; Shen, Y. R.; Quine, Z.; Romano, E.; Hartnett, D. *J. Phys. Chem. B* **2007**, *111*, 4103–4108.
(8) Pravica, M.; Grubor-Urosevic, O.; Hu, M.; Chow, P.; Liermann, P. *J. Phys. Chem. B* **2007**, *111*, 11635–11637.
(9) Breslow, R. *Acc. Chem. Res.* **1973**, *6*, 393–398.
(10) Feller, D.; Craig, N. C.; Matlin, A. R. *J. Phys. Chem. A* **2008**, *112*, 2131–2133.
(11) PierrefixeS. C. A. H. BickelhauptF. M. *J. Phys. Chem. A*, . published online May 10, http://dx.doi.org/10.1021/jp800514n.
(12) Stevenson, C. D.; Brown, E. C.; Hrovat, D. A.; Borden, W. T. *J. Am. Chem. Soc.* **1998**, *120*, 8864–8867.
(13) Andres, J. L.; Castano, O.; Morreale, A. R; Palmeiro, R.; Gomperts, R. *J. Chem. Phys.* **1998**, *108*, 203–207.
(14) Evans, W. J.; Wink, D. J.; Wayda, A. L.; Little, D. A. *J. Org. Chem.* **1981**, *46*, 3925–3928.
(15) Streitwiese, A., Jr.; Muller-Westerhoff, U. *J. Am. Chem. Soc.* **1968**, *90*, 7364.
(16) Wenthold, P. G.; Hrovat, D. A.; Borden, W. T.; Lineberger, W. C. *Science* **1996**, *272*, 1456–1459.
(17) Katz, T. J. *J. Am. Chem. Soc.* **1960**, *82*, 3784–3785.
(18) Sommerfeld, T. *J. Am. Chem. Soc.* **2002**, *124*, 1119–1124.
(19) McMillan, P. F. *Nat. Mater.* **2007**, *6*, 7–8.
(20) Ciabini, L.; Santoro, M.; Gorelli, F. A.; Bini, R.; Schettino, V.; Raugei, S. *Nat. Mater.* **2007**, *6*, 39–43.
(21) Ciabini, L.; Gorelli, F. A.; Santoro, M.; Bini, R.; Schettino, V.; Mezouar, M. *Phys. Rev. B* **2005**, *72*, 094108.
(22) Jackson, B. R.; Trout, C. C.; Badding, J. V. *Chem. Mater.* **2003**, *15*, 1820–1824.
(23) Ciabini, L.; Santoro, M.; Bini, R.; Schettino, V. *J. Chem. Phys.* **2002**, *116*, 2928–2935.
(24) Zhou, X.; Liu, R.; Pulay, P. *Spectrochim. Acta* **1993**, *49A*, 953–964.
(25) Claus, K. H.; Kruger, C. *Acta Crystallogr.* **1988**, *C44*, 1632–1634.
(26) Lippincott, E. R.; Lord, R. C.; McDonald, R. S. *J. Am. Chem. Soc.* **1951**, *73*, 3370–3383.
(27) Forman, R. A.; Piermarini, G. J.; Barnett, J. D.; Block, S. *Science* **1972**, *176*, 284–285.
(28) Hammersley, A. P.; Svensson, S. O.; Hanfland, M.; Fitch, A. N.; Hausermann, D. *H. Pres. Res.* **1996**, *14*, 235–248.
(29) Nolze, G.; Kraus, W. *Powder Diffr.* **1998**, *13*, 256–259.
(30) Delley, B. *J. Chem. Phys.* **2000**, *113*, 7756–7764. DMol3 is available as part of Materials Studio.
(31) Frish, M. J. et al. *Gaussian 03*, Rev. C.02; Gaussian Inc.: Wallingford, CT, 2004.
(32) Wang, Y.; Perdew, J. P. *Phys. Rev. B* **1992**, *45*, 13244–13249.
(33) Zhou, Z.; Zhao, J.; Chen, Z.; Gao, X.; Yan, T.; Wen, B.; Schleyer, P. v. R. *J. Phys. Chem. B* **2006**, *110*, 13363–13369.
(34) Hehre, W. J.; Radom, L.; Schleyer, P. R.; Pople, J. A. *Ab Initio Molecular Orbital Theory*; Wiley: New York, 1986.
(35) Delley, B. *J. Chem. Phys.* **1990**, *92*, 508–517.
(36) Monkhorst, H. J.; Pack, J. D. *Phys. Rev. B* **1976**, *13*, 5188–5192.

(37) Parrinello, M.; Rahman, A. *Phys. Rev. Lett.* **1980**, *45*, 1196–1199. Parrinello, M.; Rahman, A. *J. Appl. Phys.* **1981**, *52*, 7182–7190.
(38) Perdew, J. P.; Burke, K.; Ernzerhof, M. *Phys. Rev. Lett.* **1996**, *77*, 3865–3868.
(39) Troullier, N.; Martins, J. L. *Phys. Rev. B* **1991**, *43*, 1993–2006.
(40) Kim, E.; Kumar, R.; Weck, P. F.; Cornelius, A. L.; Nicol, M.; Vogel, S. C.; Zhang, J.; Hartl, M.; Stowe, A.; Daemen, L.; Zhao, Y. *J. Phys. Chem. B* **2007**, *111*, 13873–13876.
(41) Kim, E.; Weck, P.; Balakrishnan, N.; Bae, C. *J. Phys. Chem. B* **2008**, *112*, 3283–3286.
(42) Lawless, M. K.; Mathies, R. A. *J. Chem. Phys.* **1994**, *100*, 2492–2504.
(43) Tkachev, S. N.; Manghnani, M. H.; Williams, Q. *Phys. Rev. Lett.* **2005**, *95*, 057402.
(44) Tkachev, S. N.; Bass, J. D. *J. Chem. Phys.* **1996**, *104*, 10059–10060.
(45) Nicol, M.; Yin, G. Z. *J. Phys. (Paris)* **1984**, *45*, 163–172.

JP806968C